Delamination Susceptibility of Coatings Under High Thermal Flux

Z. Xue
School of Engineering and Applied Sciences,
Harvard University,
29 Oxford Street,
Cambridge, MA 02138

A. G. Evans
Department of Mechanical Engineering,
University of California,
Santa Barbara, CA 93106

J. W. Hutchinson
School of Engineering and Applied Sciences,
Harvard University,
29 Oxford Street,
Cambridge, MA 02138

Delamination of coatings initiated by small cracks paralleling the free surface is investigated under conditions of high thermal flux associated with a through-thickness temperature gradient. A crack disrupts the heat flow thereby inducing crack tip stress intensities that can become critical. A complete parametric dependence of the energy release rate and mode mix is presented in terms of the ratio of the crack length to its depth below the surface and coefficients characterizing heat transfer across the crack and across the gaseous boundary layer between the surface and the hot gas. Proximity to the surface elevates the local temperature, which in turn, may significantly increase the crack driving force. A detailed assessment reveals that the energy release rates induced by high heat flux are capable of extending subsurface delaminations in thermal barrier coatings, but only when the modulus has been elevated by either calcium-magnesium-alumino-silicate (CMAS) penetration or sintering. Otherwise, the energy release rate remains well below the toughness. [DOI: 10.1115/1.3086590]

1 Introduction

When brittle coatings function in the presence of thermal gradients and high heat flux, they are susceptible to delamination and spalling. The most widely investigated examples are thermal barrier coatings (TBCs) used in turbines for aeropropulsion and power generation. Articles that describe and analyze the mechanisms capable of providing sufficient energy release rate, G_{delam}, to drive delamination have been presented [1–4]. They are in two basic mechanism categories, governed by the sign of the stress in the coating at its surface. (i) When this stress is tensile, sufficient energy release rate of delamination cracks parallel to the surface only arises when a secondary crack perpendicular to the delamination links it to the free surface allowing the stress above the delamination to be released. Similarly, if the delamination connects to a free edge the coating can displace in mixed mode as the delamination extends [1]. The scenario providing the largest G_{delam} is that involving a temperature gradient during operation having sufficient magnitude to induce an appreciable tensile stress at the surface upon cooling to ambient [2,5]. Other mechanisms that generate tension at the surface are not sufficiently potent: these include sintering-induced stresses. (ii) When the surface is in compression, an energy release rate for an edge delamination crack still exists (albeit that it is strictly mode II). In this case, if the delamination extends to a free edge, or is connected to the surface by a wide cracklike gap, the stress in the coating above the delamination can be released as the delamination extends. In the absence of cracks linking to the surface or free edges, the energy above the delamination can be released by buckling, but this requires a large initial delamination to already exist, formed by some (independently specified) mechanism. Another potent mechanism involves rapid heat-up in the presence of a subsurface flaw (Fig. 1). In this scenario, the flaw is thermally insulting, resulting in a temperature difference, ΔT_{flaw}, between its two faces (with compression at the coating surface). This ΔT_{flaw} induces an energy release rate of the cracklike flaw. Earlier estimates [3] implied that G_{delam} was too small to be of concern when temperature boundary conditions pertain at the top and bottom of the coating set by temperatures computed assuming no flaw. However, in most TBC applications, heat transfer boundary conditions apply such that the temperature at the surface above the crack is considerably higher than in the absence of a crack, rendering this mechanism more potent. Such boundary conditions are investigated here. Indeed, in high heat flux tests, dramatic spalling of the coating has been observed during heat-up [6]. The intent of this article is to re-examine rapid heating with the new boundary conditions. The emphasis will be on relatively small flaws (less than the coating thickness) to be compatible with the foregoing observations.

The analysis to be presented regards the coating as elastic (no creep) with isotropic thermal and elastic properties. Insight will be acquired by solving a sequence of increasingly complex thermal problems (Fig. 1), starting with an isolated crack in an infinite body, followed by a crack in a semi-infinite coating, and, finally, a crack in a finite coating on a conducting substrate. The problems differ thermally from that considered previously by virtue of the heat transfer boundary condition between the hot gas and the coating surface. It will become apparent that this situation causes the material above the crack to become hotter than in the absence of the crack, thereby elevating the energy release rate. The analysis will include the presence of an initial residual stress in the coating, at ambient, again to be consistent with the practical situation.

The application of the results will be illustrated for a TBC on a superalloy substrate. The coating will have thickness, $H=1$ mm, consisting of yttria-stabilized zirconia (YSZ) deposited by air plasma spray (APS) with thermal conductivity, $k=1$ W/m K, thermal expansion coefficient, $\alpha=11$ ppm/°C, and in-plane modulus, $E=20$ GPa [5]. For coatings infiltrated by a glasslike substance due to debris ingested into the engine, such as CMAS to be discussed later, the assumption of isotropic thermal and elastic properties is probably justified. On the other hand, elastic and thermal isotropy is obviously an approximation for uninfiltrated plasma spray coatings, but necessary at this stage since details of the anisotropies are not yet available. The heat flux boundary condition at the surface has such a strong effect on the crack driving force that results based on the idealized isotropic coating provide considerable insight. Similarly, detailed knowledge of the fracture anisotropy of the coatings is not yet known although the morphology of the microstructure of plasma spray coatings is expected to
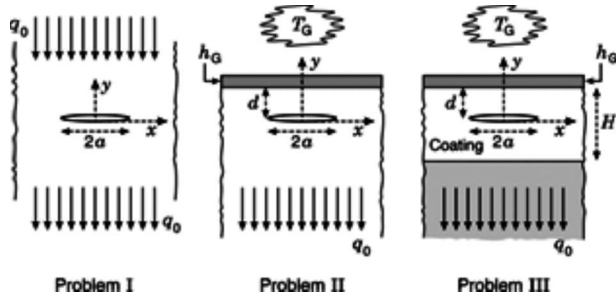
Fig. 1 Three problems analyzed in the paper. The coefficient of heat transfer across the crack is denoted by h_C in each of the three problems. The heat transfer coefficient across the gas boundary layer at the surface of the thermal barrier coating in Problems II and III (shown as a shaded layer) is denoted by h_G. The temperature of the hot gas above the boundary layer is T_G. In all three problems, the vertical heat flux in the absence of the crack is denoted by q_0.

give rise to some anisotropy, which would have some effect on delamination trajectories, as will be remarked on in the summary discussion.

2 Problem Statement

Each of the three problems depicted in Fig. 1 is infinite in extent in the x-direction. Throughout the paper, $T_0(y)$ denotes the temperature distribution in the absence of the crack. Under the steady state thermal conditions considered here, $T_0(y)$ satisfies $\nabla^2 T_0 = d^2 T_0 / d^2 y = 0$. The heat flux through the coating when no crack is present is denoted by

$$q_0 = k dT_0/dy \tag{1}$$

with k as the thermal conductivity.

Denote the heat transfer coefficient governing the thermal conduction across the crack by h_C, such that the downward thermal flux across it is $h_C(T^+ - T^-)$ expressed in terms of the temperatures on its top $(+)$ and bottom $(-)$ faces. The condition

$$k \frac{\partial T}{\partial y} = h_C(T^+ - T^-) \tag{2}$$

must be satisfied at all points with $\partial T / \partial y$ continuous across the crack. For Problems II and III, the role of heat transfer through the gaseous boundary separating the surface of the coating and the hot gas at temperature T_G is taken into account. Denote the heat transfer coefficient for the boundary layer by h_G, such that at any point along the surface with temperature T_{surface} the heat flux into the surface is

$$k \frac{\partial T}{\partial y} = h_G(T_G - T_{\text{surface}}) \tag{3}$$

The steady-state temperature distributions for the three problems in the absence of the crack are as follows. For Problem I, the heat flux, q_0, is specified

$$T_0(y) = T_0(0) + \frac{q_0 y}{k} \tag{4}$$

with $T_0(0)$ having no influence. For Problem II, both q_0 and T_G are specified

$$T_0(y) = T_{0\text{surface}} + \frac{q_0(y - d)}{k}, \quad T_{0\text{surface}} = T_G - \frac{q_0}{h_G} \tag{5}$$

For Problem III, T_G and $T_{\text{substrate}}$ are specified

$$T_0(y) = T_{0\text{surface}}\left(\frac{H - d + y}{H}\right) + T_{0\text{interface}}\left(\frac{d - y}{H}\right) \tag{6}$$

with $T_{0\text{interface}}$ as the temperature at the coating/substrate interface. The heat flux and surface temperature are

$$q_0 = \frac{\text{B}_G}{(\text{B}_G + 1 + \text{B}_G \ H_S/H)} \frac{k(T_G - T_{\text{substrate}})}{H} \tag{7}$$

and

$$T_{0\text{surface}} = T_G - \frac{q_0}{h_G}$$

where the dimensionless Biot number for the gaseous boundary layer is defined as

$$\text{B}_G = \frac{h_G H}{k} \tag{8}$$

A sense for the numerical values of the variables is provided for the TBC example cited in Sec. 1. With $T_G - T_{0\text{surface}} = 400°\text{C}$ and $T_{0\text{surface}} - T_{0\text{interface}} = 400°\text{C}$ as the temperatures drops across the boundary layer and coating, respectively, the parameters become $h_G = 1 \ \text{kW/m}^2 \ \text{K}$, $\text{B}_G = 1$, and $q_0 = 0.4 \ \text{MW/m}^2$.

Regardless of the constraint at infinity, only two nonzero thermal-stress components result from $T_0(y)$: $\sigma_{xx}(y)$ and $\sigma_{zz}(y)$. These components induce zero energy release rate for a crack parallel to the surface. Similarly, residual stresses parallel to the surface have no effect on the energy release rate of cracks parallel to the surface. *Consequently, only the temperature change, $\Delta T(x,y)$, due to the presence of the crack produces stress intensities*, where

$$\Delta T(x,y) = T(x,y) - T_0(y) \tag{9}$$

Steady-state requires $\nabla^2 \Delta T(x,y) = 0$. If the crack does not impede the heat flux $(h_C = \infty)$, then $\Delta T(x,y) = 0$ and the energy release rate is zero.

3 Isolated Crack in an Infinite Body

Results are reviewed for the plane strain problem of a crack in an infinite body (Problem I, Fig. 1) subject to a downward-directed vertical heat flux, $q_0 = k dT_0 / dy$, remote from the crack. In the limit of no heat transfer across the crack $(h_C = 0)$, a closed form solution exists [7,8]. With K_I and K_{II} denoting the mode I and II stress intensity factors, the problem is pure mode II $(K_I = 0)$, with energy release rate given by

$$G_0(0) = \frac{\pi}{16} \Omega \left(\frac{a}{H}\right)^3, \quad \Omega = \frac{EH^3 \alpha^2 q_0^2 (1 + \nu)}{k^2 (1 - \nu)} \tag{10}$$

where $2a$ is the crack length, E and ν are Young's modulus and Poisson's ratio of the material, α its coefficient of thermal expansion, and H is a characteristic dimension (later equated to the coating thickness). The rationale for the notation $G_0(0)$ will become apparent; the subscript 0 signifies an isolated crack. The result (Eq. (10)) has the notable features that the energy release rate is sensitive to crack length, $G_0 \sim a^3$, and the heat flux, $G_0 \sim q_0^2$. These strong dependencies often dominate the incidence of delamination, as elaborated later.

If $h_C \neq 0$, the problem is still pure mode II, but the energy release rate now depends on a dimensionless Biot number defined by

$$\text{B}_C^* = \frac{h_C a}{k} \tag{11}$$

This problem does not have a closed form solution. A numerical result [9] for the energy release rate is plotted in Fig. 2. Over the range of Biot numbers plotted $(0 \leq \text{B}_G^* \leq 2)$, an accurate fit to the numerical results is
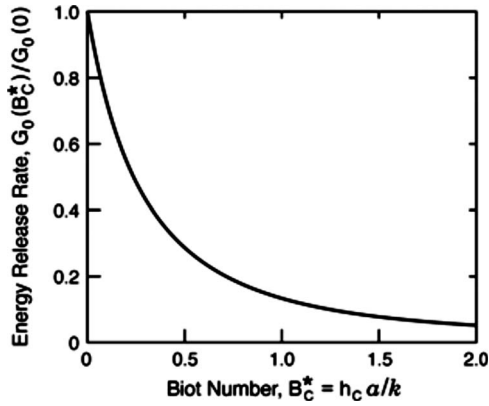
Fig. 2 Effect of heat conduction across an isolated crack on energy release rate [9]. The normalizing value $G_0(0)$ is the energy release rate for the nonconducting crack given by Eq. (10). Pure mode II pertains ($\psi=90$ deg).

$$G_0(\mathrm{B}_C^*) = \frac{G_0(0)}{\left(1 + 3.709\ \mathrm{B}_C^* + \left(\frac{\pi}{2}\mathrm{B}_C^*\right)^2\right)} \qquad (12)$$

The Poisson's ratio dependence is precisely captured through Eq. (10), and the limit for large B_C^*, $G_0(0)/(\pi\ \mathrm{B}_C^*/2)^2$, has been obtained by a rigorous perturbation expansion. A closely related result for a crack on an interface will be reported in Sec. 5. The dependence of the energy release rate on crack length is dominated by that implicit in $G_0(0)$.

4 Near-Surface Cracks in a Semi-Infinite Coating

In Problem II depicted in Fig. 1, a crack of length $2a$ lies at a depth d below the surface of the semi-infinite body. The role of heat transfer through the gaseous boundary separating the surface of the coating and the hot burning gas at temperature T_G is taken into account, as discussed in Sec. 1. The temperature distribution in the absence of the crack, $T_0(y)$, in Problem II is given by Eq. (5) with q_0 and T_G specified. In the presence of a crack, $T_0(y)$ is approached remotely from the crack. Two normalizations of the Biot number for the boundary layer will be useful

$$\mathrm{B}_G = \frac{h_G H}{k} \quad \text{and} \quad \mathrm{B}_G^* = \frac{h_G a}{k} \qquad (13)$$

The first normalization employing the layer thickness, H, was introduced in Eq. (7). Even though H does not enter directly in Problem II, B_G obtains for an actual coating, as illustrated by the estimate of B_G obtained below Eq. (8), and then $\mathrm{B}_G^*=(a/H)\mathrm{B}_G$.

Plane strain conditions governing the changes in stress and strain due to the presence of the crack are assumed. As noted earlier, only the change in temperature ΔT due to the presence of the crack generates stress intensities. Moreover, in Problem II, ΔT decays to zero remotely such that the change in remote stress is not influenced by the constraints on deformation.

4.1 The Nonconducting Shallow Crack Limit ($h_C=0$, $d/a \ll 1$). The only analytical result that has been possible to derive is the asymptotic solution for a shallow nonconducting crack ($h_C=0$, $d/a \ll 1$) (see the Appendix). The result is

$$G = \frac{1}{2}\frac{(1+\nu)}{(1-\nu)}Ed\left(\frac{\alpha q_0 a}{k}\right)^2\left[\frac{\pi}{4} + \frac{1}{\mathrm{B}_G^*}\left(1 - \frac{\tanh(\sqrt{\mathrm{B}_G^*\ a/d})}{\sqrt{\mathrm{B}_G^*\ a/d}}\right)\right]^2 \qquad (14)$$
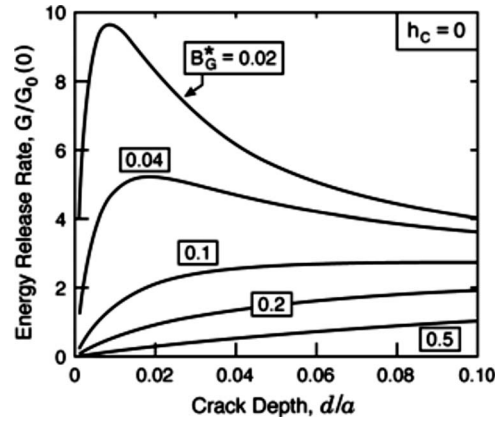
with

Fig. 3 Amplification of energy release rate for shallow cracks, as predicted by the asymptotic result for the energy release rate of a crack just below the surface as dependent on the Biot number governing heat transfer through the gas boundary layer, $\mathrm{B}_G^*=h_G a/k$. The crack length is $2a$ and the depth below the surface is d. The crack is nonconducting ($h_C=0$) and has mode mix $\psi=52.1$ deg. The normalizing value, $G_0(0)$, pertains to the isolated crack experiencing the same overall heat flux given by Eq. (10).

$$\psi = \tan^{-1}\left(\frac{K_{\mathrm{II}}}{K_{\mathrm{I}}}\right) = 52.1\ \text{deg} \qquad (15)$$

Normalizing G by $G_0(0)$ in Eq. (10) for the isolated crack of length $2a$ subject to the same overall heat flux q_0 gives

$$\frac{G}{G_0(0)} = \frac{8}{\pi}\frac{d}{a}\left[\frac{\pi}{4} + \frac{1}{\mathrm{B}_G^*}\left(1 - \frac{\tanh(\sqrt{\mathrm{B}_G^*\ a/d})}{\sqrt{\mathrm{B}_G^*\ a/d}}\right)\right]^2 \qquad (16)$$

which is plotted in Fig. 3. The most important observation is the existence of a range of shallow locations for which $G/G_0(0)$ can be significantly in excess of unity if $\mathrm{B}_G^* \equiv ah_G/k \le 0.1$. The implication is that cracks near the surface can become critical at considerably lower overall heat flux than deeper cracks. This feature arises because disruption of the heat flow substantially elevates the surface temperature just above the shallow crack. This elevation increases the compressive stress in the ligament above the crack, which, in turn, increases the energy release rate. In the extreme, the local surface temperature can approach T_G.

4.2 The Nonconducting Near-Surface Crack ($h_C=0$). Finite element thermal-stress analyses for all cases were carried out using ABAQUS/Standard software [10]. The deformation is taken to be plane strain, and the material is represented by the linear elasticity. Utilizing symmetry, only the half of the geometry to the right of the symmetry line ($x=0$) was analyzed. Symmetric boundary conditions were applied on the symmetry line. The distance to right edge is taken to be sufficiently large compared with both the crack length and the total thickness in the y-direction, such that the intensity factors are independent of this distance. The right edge is taken to be traction free. The heat transfer boundary condition on the top surface was specified through ABAQUS's thermal load option *SFILM, while a fixed uniform temperature was applied to the bottom surface. The crack was modeled as two separate surfaces with a small gap. The thermal conduction condition across the crack can be specified through ABAQUS's thermal contact option *GAP CONDUCTANCE. The meshes were devised to give highly accurate results for the energy release rate established by comparison with known results, such as those for the isolated crack in Eqs. (10) and (12). In particular, the result for the isolated crack with partial thermal conductivity in Eq. (12) and Fig. 2 was validated to within a fraction of a percent. A highly refined mesh is laid out on the ligament ahead of the tip. Eight
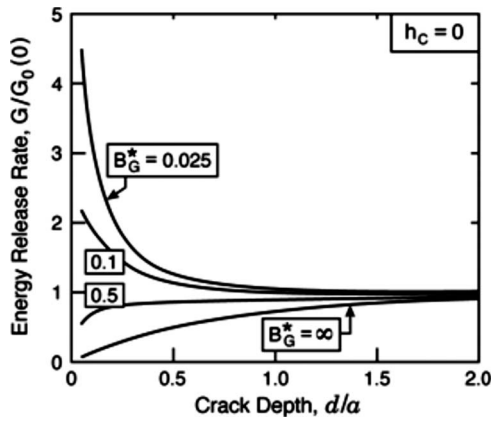
Fig. 4 Normalized energy release rate computed numerically for nonconducting crack of length $2a$ located a distance d below the surface for various Biot numbers, $B_G^* = h_G a/k$, characterizing the gaseous boundary layer at the surface. The normalizing value, $G_0(0)$, pertains to the isolated crack experiencing the same overall heat flux given by Eq. (10), i.e., the limit $d/a \gg 1$.

node quadrilateral elements with reduced integration were employed for the fully coupled thermal-stress analyses. Such elements exploit the biquadratic shape function for the displacement and a bilinear shape function for the temperature. The crack tip was modeled with a ring of collapsed quadrilateral elements to capture the strain singularity, thus improving the accuracy of the calculations, (see ABAQUS manual for details). At the crack tip, the elemental size is on the order of one-hundredth of the crack depth.

Numerical results for G and ψ computed for $0.05 \leq d/a \leq 2$ and selected B_G^* are plotted in Figs. 4 and 5. They affirm the trends exposed by the asymptotic formulas, Eqs. (14) and (15), and reveal that cracks with $d/a < 1/2$ can experience energy release rates well above those for deep cracks if $B_G^* \leq 0.1$. It appears that the mode mix, ψ, is independent of B_G^*, but it has not been possible to establish this theoretically. The numerical results establish the range of validity of the asymptotic formulas is limited to $d/a \leq 0.1$.

The elevation of the energy release rate due to surface proximity only arises when there is a substantial temperature drop across the gaseous boundary layer (small B_G^*). Conversely, when $B_G^* \to \infty$ such that $T_{\text{surface}} = T_G$, the boundary layer is eliminated, and
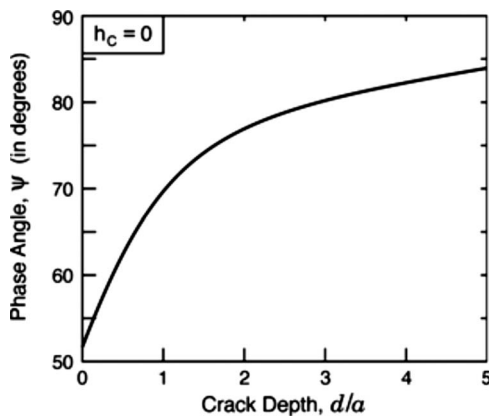

Fig. 5 Mode mix, ψ, computed numerically for nonconducting crack of length $2a$ located a distance d below the surface. The curve applies to all Biot numbers, $B_G^* = h_G a/k$, characterizing the gaseous boundary layer at the surface. This result also applies for Problem II for any combination of B_C^* and B_G^*.
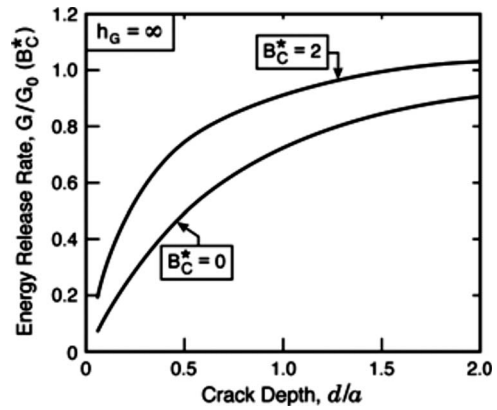

Fig. 6 Normalized energy release rate computed numerically for limit ($h_G = \infty$ and $T_{\text{surface}} = T_G$) with no gaseous boundary layer. The Biot number governing heat transfer across the crack is $B_C^* = h_C a/k$, and $G_0(B_C^*)$ is given by Eq. (12). The mode mix, ψ, is plotted in Fig. 5.

surface proximity reduces the energy release rate. The transition occurs for $B_G^* \cong 0.25$, where G is essentially independent of the crack depth.

For completeness results for the limit $h_G = \infty$, $T_{\text{surface}} = T_G$ is plotted in Fig. 6, affirming that proximity to the surface reduces G relative to that for the deep crack.

4.3 The Near-Surface Crack With Combinations of h_C and h_G. Selected results in Fig. 7 illustrate how the thermal conductivities of the boundary layer and the crack interact to determine the energy release rate. The plot quantifies trends that would be expected from the previous plots when either the crack is nonconducting or the boundary layer provides no thermal resistance. Specifically, elevation of the energy release rate due to proximity to the surface depends on both B_C^* and B_G^*. For $B_C^* = 0.2$, appreciable elevation near the surface only occurs if $B_G^* \leq 0.1$. For $B_C^* = 0.5$, it does not occur for any $B_G^* \geq 0.025$ (plot not shown).

5 Cracks in a Coating on a Substrate

When the crack is short ($a/H \ll 1$) and relatively near the surface, the results of Sec. 4 apply. Otherwise, for Problem III, interaction with the substrate must be taken into account. In thermal barrier systems, the conductivity of the metal substrate is typically at least over an order of magnitude greater that of the coating, enabling the temperature along the bottom surface of the sub-
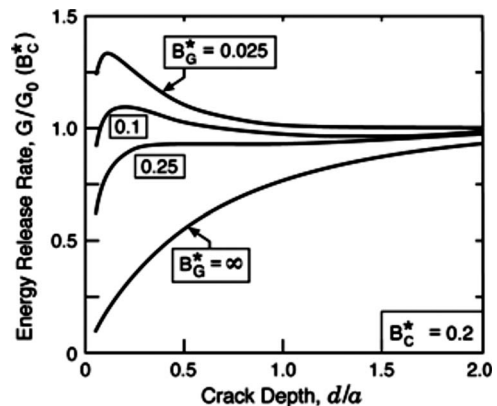

Fig. 7 Normalized energy release rate computed numerically for $B_C^* = h_C a/k = 0.2$ and various $B_G^* = h_G a/k$ with $G_0(B_C^*)$ given by Eq. (12). The mode mix, ψ, is plotted in Fig. 5.
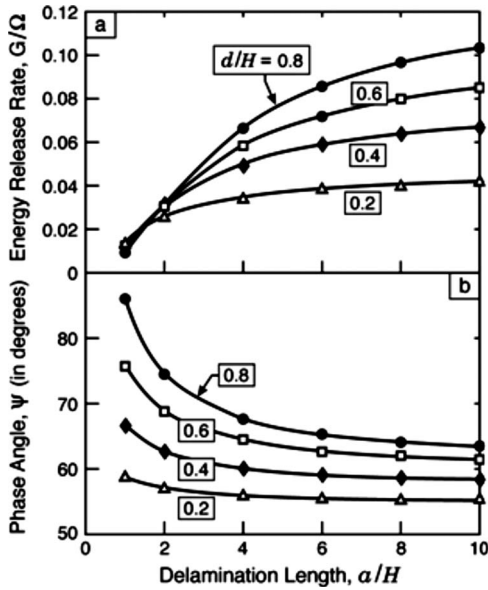
Fig. 8 Energy release rate and mode mix in Problem III computed numerically for cracks at various depths for $B_C = 0$ and $B_G = 1$. $H_S/H = 3$, $k_{substrate}/k = 100$, $E_{substrate}/E = 5$, $\nu_{substrate} = 0.3$, and $\nu_{TBC} = 0.2$.

Fig. 9 Energy release rate computed numerically for shallow cracks at various depths for $B_C = 0$ and $B_G = 1$ for $q_0 = 0.4$ MW/m² and $E = 200$ GPa ($H = 1$ mm, $k = 1$ W/m K, $\nu = 0.2$, and $\alpha = 11 \times 10^{-6}$/K). Critical flaw sizes are indicated based on a representative mode I toughness, Γ_{TBC}.

strate, $T_{substrate}$, to be nearly uniform. Interaction of a relatively short, deep crack ($a/H \ll 1$) with the substrate significantly reduces the energy release rate. Detailed trends will not be presented, rather, one result will be quoted in Sec. 5.1.

5.1 Short Crack ($a/H \ll 1$) at the Interface With the Substrate. Consider a plane strain crack of length $2a$ on the interface between two semifinite half spaces. The half space above the interface has moduli, coefficient of thermal expansion, and thermal conductivity taken to be the same as those in Problem I. The half space below the interface has identical moduli to that above the interface with an infinite thermal conductivity (recall that the thermal conductivity of the metal substrate is typically ten times that of the coating). The remote heat flow is q_0 and the heat transfer across the crack is h_C, as before.

It has not been possible to find the solution to this problem in literature, although a general solution for the interface crack with zero conductivity is available [11]. It is relatively straightforward to show that this problem with nonzero h_C is pure mode II, and that the stress intensity factor, K_{II}, is exactly half that for the isolated crack of length $2a$ in the uniform material (Problem I), except that the corresponding heat transfer coefficient across the crack must be taken as $2h_C$. (Solution details are omitted.) Thus, the short interface crack has a greatly reduced energy release rate given precisely by

$$G = \frac{1}{4}G_0(2 \ B_C^*)$$ (17)

where G_0 is give by Eq. (12). The result holds in the limit when there is no heat conducted across the crack, $h_C = 0$, and agrees with the result in Ref. [11]. It does not depend on the coefficient of thermal expansion of the lower half space.

5.2 Long Crack ($a/H \gg 1$). Numerical results for Problem III are presented in Fig. 8 for the specific case of a substrate with $H_S/H = 3$, $k_{substrate}/k = 100$, $E_{substrate}/E = 5$, and $\nu_{substrate} = 0.3$. The result depends on Poisson's ratio of the coating, taken as $\nu = 0.2$. The two relevant Biot numbers are defined as $B_C = h_C H/k$ and $B_G = h_G H/k$. The energy release rate can be expressed in the form
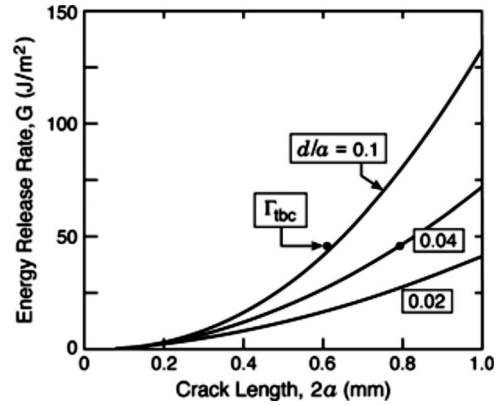
$$G = \Omega F(a/H, d/H, B_G, B_C)$$ (18)

where F is a dimensionless function of the arguments shown. The trend with the normalized depth for a nonconducting crack ($B_C = 0$) reveals that the surface enhancement of G only occurs for the shallow cracks considered in Sec. 3. For long cracks ($a/H \gg 1$), G increases with depth below the surface. In all cases, G increases and ψ decreases with crack extension, although the asymptotic limit for very long cracks is nearly attained for $a/H = 10$. The implication is that any crack that attains modest length, $a/H \approx 1$, once critical, will propagate unstably without arrest.

6 Implications

The application of the foregoing results is illustrated for a YSZ-TBC on a superalloy substrate. The coating has thickness, $H = 1$ mm, with thermal conductivity, $k = 1$ W/m K, thermal expansion coefficient, $\alpha = 11$ ppm/°C, and in-plane modulus, $E = 20$ GPa [5]. The initial examples regard the temperatures drops across the boundary layer and coating as, respectively, $T_G - T_{0surface} = 400$°C and $T_{0surface} - T_{0interface} = 400$°C. Other values are invoked as the arguments emerge. The ensuing thermal parameters are $h_G = 1$ kW/m² K, $B_G = 1$, and $q_0 = 0.4$ MW/m². This set of parameters results in an energy release rate coefficient, $\Omega \approx 580$ J m⁻². While this is quite large relative to the mode I toughness of the TBC ($\Gamma \approx 50$ J m⁻²) [12,13], note that the actual energy release rate is much smaller because of qualifying terms substantially less than unity, as elaborated below. A preamble before proceeding is that the phase angle, in all cases, is in the range $50 \le \psi \le 90$ deg. Consequently for a medium with isotropic fracture resistance, the crack would extend diagonally down through the coating (not parallel to the substrate). Fracture anisotropy, if sufficient, could result in parallel delaminations, but this seems unlikely given the degree of mode mixity unless the anisotropy is quite large. The exception is delaminations in the coating just above the substrate. These could oscillate in the coating as they extend (on average) parallel to the surface, in accordance with the appropriate mixed mode toughness. Given that this situation is the most realistic, it is considered first. The preliminary estimates assume an insulating crack ($h_c = 0$) to obtain the maximum possible energy release rates.

The most basic result is the trend in $G_0(0)$ as a function of crack length, ascertained for 50 μm $\le 2a \le 1$ mm, for various levels of heat flux within the range $0.4 \le q_0 \le 2$ MW/m² (Fig. 9). To interpret these plots, the fracture toughness must be superposed. For this purpose, the mode I toughness of YSZ ($\Gamma \approx 50$ J m⁻²) [12,13] has been included in the figure. This choice
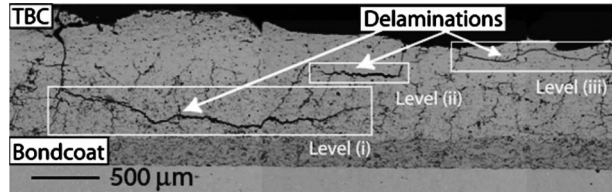
Fig. 10 Delaminations in the TBC on an engine shroud [5]. The delaminations just below the surface occur within the CMAS infiltrated regions, which give rise to a significantly increased Young's modulus.

Fig. 11 (a) Cut above the crack creating a simply connected region. (b) Resultant force/length and moment/length required to eliminate displacement discontinuity across the cut in (a).

again represents a worst case from a delamination susceptibility perspective, since the delaminations are mixed mode with appreciably higher toughness. Recall that, for short cracks, $G = G_0(0)/4$, it is apparent that, even at the highest heat flux, the energy release rate only becomes sufficiently large to attain the toughness when the delaminations exceed about 1 mm in length ($a/H > 1$). The same conclusion is reached by referring to Fig. 7, recalling that $\Omega \approx 580$ J m^{-2}. Such long cracks do not pre-exist in these systems, but could form due to other thermomechanical phenomena [1,5,14]. Once delaminations of this length have been created just above the substrate, the heat flux induced energy release rate would lead to catastrophic extension, with associated spalling.

The situation for short cracks just below the surface can be judged by combining the information contained in Figs. 3, 4, and 7 with that in Fig. 8. An example is presented for short cracks, $0.1 \le a/H \le 0.5$, just beneath the surface, $0.01 \le d/a \le 0.1$. The result for a representative flux, $q_0 = 0.4$ MW/m^2, and a conventional choice of the modulus ($E = 20$ GPa) indicates that G always remains below the mode I toughness. The corresponding result for a case wherein the top of the TBC has either sintered or been filled with CMAS ($E = 200$ GPa) is plotted in Fig. 9. For this case, G can exceed Γ for shallow cracks in the length and depth ranges $2a \approx 0.6$ mm and $d \approx 30$ μm. Namely, moderately long shallow cracks are susceptible to delamination. Moreover, recalling that increasing the heat flux by a factor 1.5 would increase G by a factor 2.25 (because of the scaling, $\Omega \sim q_0^2$) infers that situations capable of generating an extreme heat flux would allow short shallow cracks to delaminate. Indeed, delaminations of this type reported in CMAS infiltrated airfoils (type (iii) in Fig. 10) [5] had previously defied explanation. In summary, high heat flux appears to be capable of extending subsurface delaminations, but only when the modulus has been elevated by either CMAS penetration or sintering. Otherwise, the energy release rates remain well below the toughness, unless large delaminations have already formed by other mechanisms.

Acknowledgment

Appendix: Asymptotic Analysis for Shallow Nonconducting Cracks—Problem II

Problem II in Fig. 1(b) in the limit $d/a \ll 1$ is considered for plane strain cracks with $h_C = 0$. The first step in the analysis is to obtain the temperature distributions above and below the crack. Because the layer above the crack is thin and because no heat is conducted across the crack, the y-dependence of the temperature in this layer is negligible. Conservation of heat under the steady-state conditions of interest requires
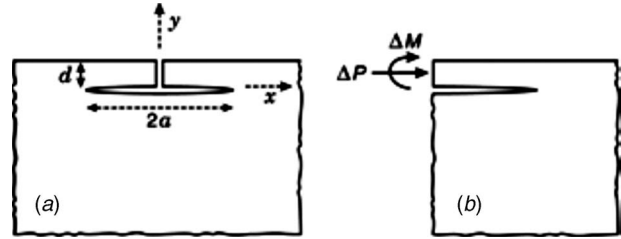
$$\frac{d^2T}{dx^2} - \frac{h_G}{kd}T = -\frac{h_G}{kd}T_G, \quad |x| < a, \quad 0 \le y \le d \qquad \text{(A1)}$$

Zones whose size is of order d exist at the ends of the crack, in which the temperature transitions from that in the strip to the surface temperature $T_{0\text{surface}}$ are given by Eq. (5). This zone shrinks to zero as d/a becomes small. These zones are ignored and the boundary conditions for Eq. (A1) are taken as $T(\pm a) = T_{0\text{surface}}$. Thus, the temperature distribution above the crack is

$$T = T_G - \frac{q_0}{h_G} \frac{\cosh(\sqrt{B_G^* \, a/d} \, x/a)}{\cosh\sqrt{B_G^* \, a/d}}, \quad |x| < a, \quad 0 \le y \le d$$

$$\text{(A2)}$$

An approximation to the temperature distribution on the bottom surface of the crack also exploits the facts that the crack is thermally insulating and $d/a \ll 1$. Consider the thermal problem for the half space below the crack line along $y = 0$. For $|x| < a$, $\partial T/\partial y = 0$. For $|x| > a$, $T = T_0(0)$, where $T_0(0)$ is given by Eq. (5), with transition zones of order d between these two conditions at the crack ends. If these zones are ignored, the conditions along $y = 0$ are identical to those for the classical problem of an isolated nonconducting crack subject to remote heat flux, q_0, in an infinite plane. The temperature distribution just below the crack is

$$T = T_0(0) - \frac{q_0 a}{k}\sqrt{1 - \left(\frac{x}{a}\right)^2}, \quad |x| < a, \quad y = 0^- \qquad \text{(A3)}$$

The change in temperature due to presence of the crack, $\Delta T = T - T_0(y)$, determines the stress intensity factors

$$\Delta T = \frac{q_0}{h_G}\left[1 - \frac{y}{a}B_0^* - \frac{\cosh(\sqrt{B_G^* \, a/d}\, x/a)}{\cosh\sqrt{B_G^* \, a/d}}\right], \quad |x| < a, \quad 0 \le y \le d$$

$$\text{(A4)}$$

$$\Delta T = -\frac{q_0 a}{k}\sqrt{1 - \left(\frac{x}{a}\right)^2}, \quad |x| < a, \quad y = 0^- \qquad \text{(A5)}$$

Because the temperature change ΔT satisfies Laplace's equation, the associated strains generated under plane strain

$$\varepsilon_{xx} = \varepsilon_{yy} = \alpha(1 + \nu)\Delta T, \quad \varepsilon_{xy} = 0 \qquad \text{(A6)}$$

are compatible, producing no stress within the simply connected region shown in Fig. 11, a created by a cut along the y-axis above the crack. However, the displacements derived from these strains are discontinuous across the cut—it is the enforcement of their continuity that generates the stresses and stress intensity factors that arise from ΔT. The second step in the analysis is to compute the displacement discontinuity and then to determine the force/length, ΔP, and moment/length, ΔM, in Fig. 11(b). These are directly linked to the stress intensity factors by [15]

$$K_\text{I} = \frac{1}{\sqrt{2d}}[\Delta P \cos \omega + 2\sqrt{3}\Delta M d^{-1} \sin \omega]$$

$$K_{\mathrm{II}} = \frac{1}{\sqrt{2}d}[\Delta P \sin\omega - 2\sqrt{3}\Delta M d^{-1}\cos\omega] \qquad (A7)$$

where $\omega = 52.1$ deg.

Given the symmetry of ΔT with respect to x and the fact that the associated shear strain, ε_{xy}, vanishes, one can readily show that the displacements derived from the strains in Eq. (A6) are such that u_y is continuous across the cut, while the discontinuity of u_x varies linearly across the cut. Denote the discontinuity across the cut by $[u_x] = 2\delta + 2\theta(0^+)y$, where $\theta(0^+)$ is the rotation of the cut surface on the right, taken as positive in the clockwise sense. The difference in average strain ε_{xx} from Eq. (A6) on the top and bottom surfaces of the crack obtained using Eqs. (A4) and (A5) gives

$$\frac{\delta}{a} = -\frac{(1+\nu)\alpha q_0}{h_G}\left[\mathrm{B}_G^*\left(\frac{\pi}{4} + \frac{d}{a}\right) + 1 - \frac{\tanh\sqrt{\mathrm{B}_G^*\ a/d}}{\sqrt{\mathrm{B}_G^*\ a/d}}\right] \quad (A8)$$

The rotation discontinuity is given by $\theta(0^+) = \theta(a) + \int_0^a \kappa\,dx$, where $\theta(a)$ is the rotation at the right hand crack tip and κ is the curvature of the upper crack surface. Because ΔT varies linearly with y in the layer above the crack in Eq. (A4), the latter is immediately obtained using Eq. (A6) with

$$\kappa = \frac{(1+\nu)\alpha q_0}{k} \qquad (A9)$$

Next, $\theta(a)$ can be obtained using the fact that $\partial\theta/\partial x = u_{x,xy} = (1+\nu)\alpha\,\partial\Delta T/\partial x$ along the lower surface of the crack because $\varepsilon_{xy} = 0$. Then, because symmetry dictates that the rotation vanishes at $x = 0$ below the crack, one obtains from Eq. (A5)

$$\theta(a) = -\frac{(1+\nu)\alpha q_0 a}{k} \qquad (A10)$$

Together, Eqs. (A9) and (A10) give

$$\theta(0^+) = 0 \qquad (A11)$$

The final step in the analysis is to enforce continuity of displacements across the cut by imposing ΔP and ΔM in Fig. 11(b). For slender layers $(d/a \ll 1)$, the layer can be modeled as a plate clamped at its right end. The choices

$$\Delta P = -\frac{Ed}{(1-\nu^2)}\frac{\delta}{a} = \frac{E\alpha q_0 d}{(1-\nu)h_G}\left[\mathrm{B}_G^*\left(\frac{\pi}{4} + \frac{d}{a}\right) + 1\right.$$
$$\left. -\frac{\tanh\sqrt{\mathrm{B}_G^*\ a/d}}{\sqrt{\mathrm{B}_G^*\ a/d}}\right], \quad \Delta M = 0 \qquad (A12)$$

provide continuity by canceling δ in Eq. (A8) and $\theta(0^+)$ in Eq. (A11). Then, by Eq. (A7)

$$(K_{\mathrm{I}}, K_{\mathrm{II}}) = \frac{E\sqrt{d}}{\sqrt{2}(1-\nu)}\frac{\alpha q_0 a}{k}\left[\frac{\pi}{4} + \frac{d}{a} + \frac{1}{B_G^*}\left(1 - \frac{\tanh\sqrt{\mathrm{B}_G^*\ a/d}}{\sqrt{\mathrm{B}_G^*\ a/d}}\right)\right]$$
$$\times(\cos\omega, \sin\omega) \qquad (A13)$$

The term d/a in the square brackets above is negligible over the range of validity of Eq. (A13) and is on the order of terms already neglected in the analysis, thus it can be neglected. The results for G in Eq. (14) and ψ in Eq. (15) follow directly.

References

[1] Choi, S. R., Hutchinson, J. W., and Evans, A. G., 1999, "Delamination of Multilayer Thermal Barrier Coatings," Mech. Mater., **31**, pp. 431–447.

[2] Rabiei, A., and Evans, A.G., 2000, "Failure Mechanisms Associated With the Thermally Grown Oxide in Plasma-Sprayed Thermal Barrier Coatings," Acta Mater., **48**, pp. 3963–3976.

[3] Hutchinson, J. W., and Evans, A. G., 2002, "On the Delamination of Thermal Barrier Coatings in a Thermal Gradient," Surf. Coat. Technol., **149**, pp. 179–184.

[4] Evans, A. G., and Hutchinson, J. W., 2007, "The Mechanics of Coating Delamination in Thermal Gradients," Surf. Coat. Technol., **201**, pp. 7905–7916.

[5] Kraemer, S., Faulhaber, S., Chambers, M., Clarke, D. R., Levi, C. G., Hutchinson, J. W., and Evans, A. G., 2008, "Mechanisms of Cracking and Delamination Within Thick Thermal Barrier Systems in Aero-Engines Subject to Calcium-Magnesium-Alumino-Silicate (CMAS) Penetration," Mater. Sci. Eng., A, **490**, pp. 26–35.

[6] Johnson, C. A., 2007, GE Global Research Center, private communication.

[7] Florence, A. L., and Goodier, J. N., 1960, "Thermal Stress Due to Disturbance of Uniform Heat Flow," ASME J. Appl. Mech., **27**, pp. 635–639.

[8] Sih, G. C., 1963, "On the Singular Character of Thermal Stresses Near a Crack Tip," ASME J. Appl. Mech., **28**, pp. 587–589.

[9] Kuo, A. Y., 1990, "Effects of Crack Surface Heat Conductance on Stress Intensity Factors," ASME J. Appl. Mech., **57**(2), pp. 354–358.

[10] HKS, 2005, *ABAQUS/Standard User's Manual*, 6.5 ed., HKS, Providence, RI.

[11] Lee, K. Y., and Park, S.-J., 1995, "Thermal Stress Intensity Factors for Partially Insulated Interface Crack Under Uniform Heat Flow," Eng. Fract. Mech., **50**, pp. 475–482.

[12] Mercer, C., Williams, J. R., Clarke, D. R., and Evans, A. G., 2007, "On a Ferroelastic Mechanism Governing the Toughness of Metastable Tetragonal-Prime (t′) Yttria-Stabilized Zirconia ," Proc. R. Soc. London, Ser. A, **463**, pp. 1393–1408.

[13] Lampenscherf, S., 2006, Siemens AG, private communication.

[14] Johnson, M., Ruud, C. A., Bruce, J. A., and Wortman, D., 1998, "Relationships between Residual Stress, Microstructure and Mechanical Properties of Electron Beam Physical Vapor Deposition Thermal Barrier Coatings," Surf. Coat. Technol., **108–109**, pp. 80–85.

[15] Hutchinson, J. W., and Suo, Z., 1992, "Mixed Mode Cracking in Layered Materials," Adv. Appl. Mech., **29**, pp. 63–191.